Improved Wear Resistance of Low Carbon Steel by Duplex Surface Treatment Combining Cathodic Plasma Electrolytic Nitrocarburising and Anodic Plasma Electrolytic Polishing

S. A. Kusmanov[1] · I. V. Tambovskiy[1] ·
T. L. Mukhacheva[1] · I. A. Kusmanova[1] ·
S. S. Korableva[1] · I. S. Gorokhov[1]

Abstract A technology for duplex plasma treatment of the steel surface is proposed. At the first stage, it is proposed to carry out nitrocarburising at the cathode polarity of the treated sample to harden the surface layer. The composition and structure of nitrocarburised layers have been studied. It is shown that as a result of the simultaneous diffusion of nitrogen and carbon, their diffusion coefficients increase, contributing to the achievement of concentrations up to $0.74 \pm 0.14\%$ and $0.67 \pm 0.18\%$, respectively, as well as an increase in the microhardness of the surface layer to 1020 ± 20 HV. At the second stage, it is proposed to carry out anodic polishing of the nitrocarburised surface to remove the porous oxide layer with a highly developed relief, which is formed as a result of exposure to the surface of electrical discharges and high-temperature oxidation. Tribological tests have shown a joint positive effect of the hardness of the diffusion layer and low surface roughness, including a dense layer of iron oxides, on a reduction in the friction coefficient by a factor of 2 and weight wear by a factor of 23 during fatigue wear of the treated sample under boundary friction and plastic contact with the counterbody.

1 Introduction

Great attention has been paid to increasing the wear resistance of various products, assemblies and mechanisms throughout the development of engineering and technology. Among the existing technologies for increasing wear resistance, a special role is given to surface methods of processing materials. These technologies include plasma electrolytic treatment, which include plasma electrolytic oxidation [1–4], polishing [1, 5], and chemical–thermal treatment [1, 6]. Protective oxide coatings are formed at plasma electrolytic oxidation, the surface microgeometry is leveled by removing protruding irregularities at polishing, and the use of chemical–thermal treatment is aimed at creating diffusion layers of increased hardness and blocking the destruction of the material under the influence of external factors. In the latter case, processing is usually classified according to the polarity of the workpiece into cathodic and anodic options.

During anodic chemical–thermal treatment, the formation of diffusion-hardened layers occurs with the simultaneous occurrence of competing processes of diffusion, high-temperature oxidation, and anodic dissolution, which will determine the intensity of diffusion saturation, morphology, and surface properties [7]. It is the anodic dissolution of the material, which underlies plasma electrolytic polishing (PEP), which leads to a decrease in surface roughness [8].

✉ S. A. Kusmanov
sakusmanov@yandex.ru

I. V. Tambovskiy
ramstobiliti@gmail.com

T. L. Mukhacheva
mukhachevatl@mail.ru

I. A. Kusmanova
maly.s@rambler.ru

S. S. Korableva
korablewa.sveta@mail.ru

I. S. Gorokhov
isgorokhov@yandex.ru

1 Kostroma State University, 17 Dzerzhinskogo Street, Kostroma 156005, Russia

Unlike anode technologies, during cathodic treatment, there is no anodic dissolution of the surface, but its erosion occurs due to the action of electrical discharges. During anodic, as well as cathodic surface treatment, an oxide layer is formed in aqueous electrolytes. The action of electrical discharges during cathodic processes favors the growth of surface roughness. For example, this trend was observed during nitrocarburising of medium carbon [9] and stainless [10, 11] steels in carbamide electrolytes. The consequence of an increase in surface roughness may be a change in its tribological characteristics. Thus, a 1.5-fold decrease in resistance to abrasive wear was revealed during cathodic nitriding of high-speed steel R6M5 [12] and structural steel 34CrNi1Mo [13]. At the same time, cathodic nitrocarburising of low-carbon steel, which occurs at higher temperatures than nitriding, leads to increased wear resistance [14], while the surface roughness increases by an order of magnitude [15]. In the case of anodic treatment, due to anodic dissolution, the surface roughness decreases. This makes it possible to reduce the coefficient of friction and wear resistance, which was shown during anodic boriding, nitriding and nitrocarburising of carbon steels [16].

One of the solutions to the problem of increasing the wear resistance of the surface after cathodic treatment is the use of PEP as a subsequent operation after diffusion saturation. It is assumed that the removal of the resulting surface irregularities, fragile areas of the oxide layer will help reduce the friction coefficient and wear. The use of PEP oxide-diffusion coatings had a positive experience in the combined anodic nitriding and polishing of medium carbon steel samples in plasma electrolysis [17].

The purpose of this work is to study the possibility of increasing the wear resistance of low-carbon steel by duplex surface treatment combining cathodic plasma electrolytic nitrocarburising (PENC) and anodic PEP.

2 Materials and Methods

2.1 Samples Processing

Cylindrical samples of low-carbon steel (0.2 wt.% C) 10 mm in diameter, 15 mm in height and 1.00 ± 0.10 μm the surface roughness (Ra) were subjected to duplex surface treatment including cathodic PENC and subsequent anodic PEP. The cathodic PENC was carried out at the sample temperature of 850 °C, the voltage of 94 V at a current strength of 14.4 A during 5, 10, 20, and 30 min in carbamide (20 wt.%) and ammonium chloride (5 wt.%) solution (the electrolyte temperature of 30 ± 2 °C, the flow rate of 2.5 L/min) using electrolyser [18]. The anodic PEP was carried out at a voltage of 325 V at a current strength of 2 A during 1 and 2 min in ammonium sulfate (5 wt.%) solution (the electrolyte

temperature of 70 ± 2 °C, the flow rate of 1 L/min) in the same electrolyser.

2.2 Surface Characterization

Quanta 3D 200i scanning electron microscopy (FEI Company) (SEM) with an energy-dispersive spectroscope was used to observe the structure of the surface layer of the samples and for the subsequent elemental microanalysis after polishing and etching with the use of a 4% nitric acid solution in ethanol for 5–10 s. Micromed MET optical metallographic microscope with digital image visualization served to study the surface morphology. The microhardness of the surface layer was measured using a Vickers microhardness tester (Falcon 503) under a 0.1-N load. TR-200 profilometer served to study the surface roughness. The weight of samples was measured using a CitizonCY224C electronic analytical balance.

Since cylindrical samples were used in the work and the lateral surface was subjected to research, the "shaft-block" friction scheme was used in friction tests [19]. The counter body was made of tool alloy steel (wt.%: 0.9–1.2 Cr, 1.2–1.6 W, 0.8–1.1 Mn, 0.9–1.05 C) with a hardness of 65 HRC. The friction tracks images were obtained using a Quanta 3D 200i scanning electron microscope. The elemental composition on the friction track was determined using energy-dispersive spectroscopy. The temperature was measured with an MLX90614 infrared thermometer on the friction tracks directly at the exit from the friction contact zone. Friction tests were carried out in dry friction mode under a load from 10 to 85 N. The sliding speed of the sample along the counter body varied from 1.555 to 5.184 m/s. The studied range of load and sliding speed were determined by the capabilities of the friction machine. The friction path was 1000 m. When testing at each test point, 3 samples were used.

3 Results and Discussion

3.1 Formation Kinetics, Composition, Structure, and Microhardness of Diffusion Layers

Figure 1 shows the cross section of the sample after its diffusion saturation with nitrogen and carbon by PENC. The surface layers are enriched with iron oxides (Fig. 1, zone 1) due to high-temperature oxidation in water vapor, which is the main component of the vapor–gas envelope that separates the part from direct contact with the electrolyte. Electrochemical oxidation also contributes to the formation of iron oxides on the sample surface. Under the layer with iron oxides, there is a light layer with a high content of nitrogen and carbon, which may contain iron nitrides and carbonitrides. EDX analysis data (Fig. 2 and
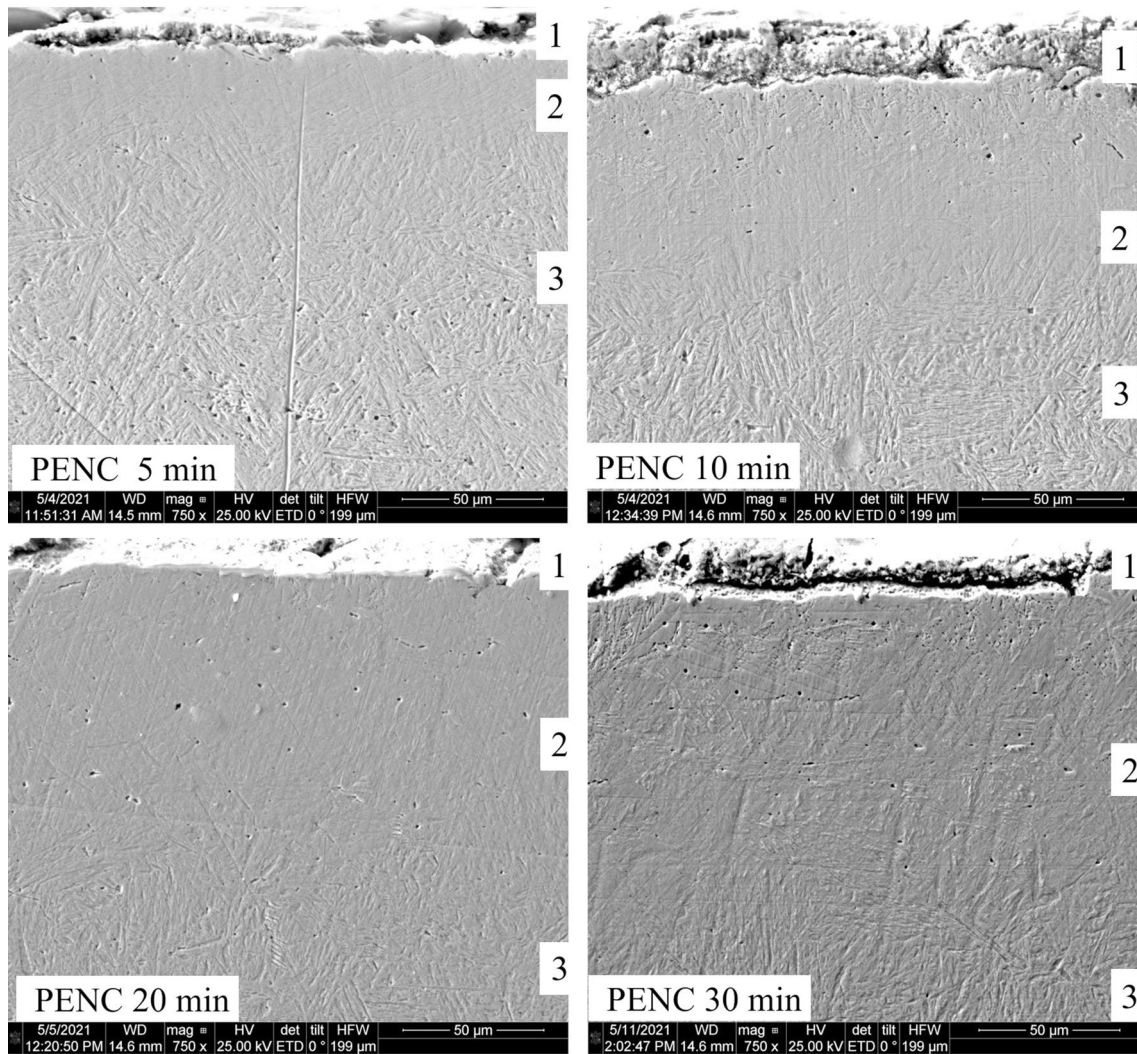
Fig. 1 SEM image of cross section of the steel surface after cathodic PENC for 5, 10, 20, and 30 min. 1—oxide layer; 2—diffusion nitrocarburised layer; 3—initial structure
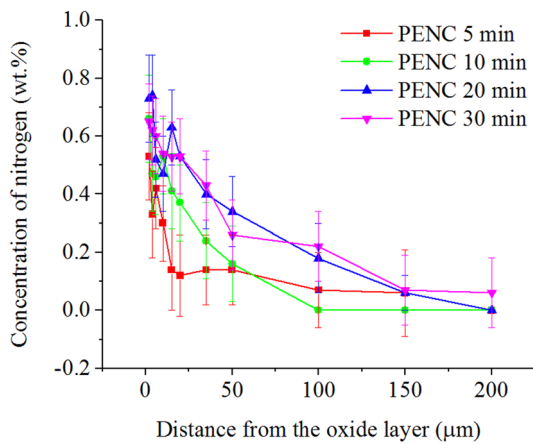

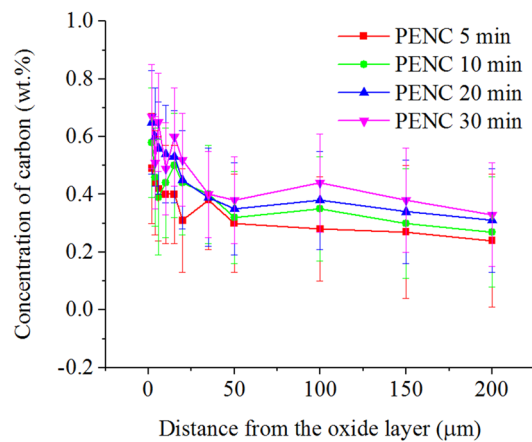**Fig. 2** EDX nitrogen distributions in the nitrocarburised layer after cathodic PENC for 5, 10, 20, and 30 min

Fig. 3 EDX carbon distributions in the nitrocarburised layer after cathodic PENC for 5, 10, 20, and 30 min
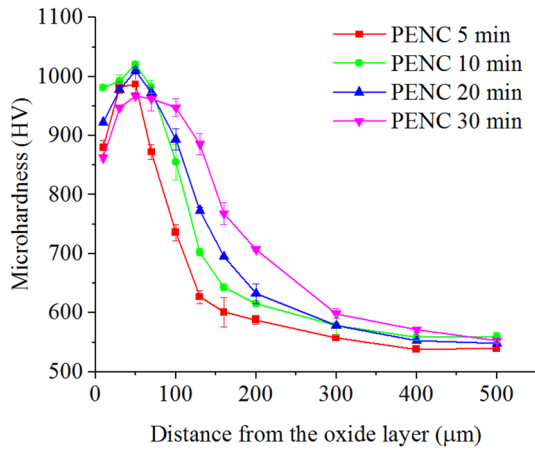
Fig. 4 Microhardness distribution in the nitrocarburised layer after cathodic PENC for 5, 10, 20, and 30 min

3) confirm an increase in the content of nitrogen and carbon after plasma electrolytic treatment over the entire temperature range. Layer 2 also contains residual austenite, as seen in Fig. 4. The maximum microhardness has shifted from the sample edge, which is typical for nitrocarburised layers. The maximum microhardness falls on the hardened region of nitrogenous fine needle martensite.

The thickness of the nitrocarburised layer increases with an increase in treatment time (Fig. 1). The concentration of nitrogen and carbon and the depth of their diffusion into the sample surface also increase with increasing diffusion saturation time to $0.67 \pm 0.18\%$ and $0.74 \pm 0.14\%$ for carbon and nitrogen, respectively.

Nitrogen and carbon concentration profiles obtained by EDX analysis make it possible to calculate the diffusion coefficients of nitrogen and carbon into the sample.

Nitrogen and carbon in the iron matrix form interstitial solid solutions. In interstitial solid solutions, in contrast to substitutional solid solutions, one can neglect the mutual influence of flows of atoms of diffusants of different types on each other's diffusion. Therefore, we will assume that the diffusion of nitrogen and carbon occurs independently. The flow of nitrogen atoms can neither accelerate nor slow

$$\frac{\partial C(x,\tau)}{\partial \tau} = D\frac{\partial^2 C(x,\tau)}{\partial x^2} , \tag{1}$$

where C is the concentration of diffusible nitrogen or carbon (wt. %); x is horizontal coordinate (m); τ is time (s); D is the diffusion coefficient (m²/s). The followings are chosen as the initial and boundary conditions:

$$\begin{aligned} C(x,0) &= C^0, \\ C(0,\tau) &= C^S, \\ C(\infty,\tau) &= C^0, \end{aligned} \tag{2}$$

where C^0 is the initial concentration of the element in the sample material, C^S is the concentration of the element on the sample surface.

The solution of Eq. (1) with conditions (2) through the error function has the form:

$$C(x,\tau) = C^S - (C^S - C^0)erf\frac{x}{2\sqrt{D\tau}} . \tag{3}$$

The diffusion coefficients are determined from Eqs. (3) for the entire set of experimental points by the least squares method.

The essence of the method is to minimize the sum of the squared deviations of the theoretical concentration values calculated by Eq. (3) from the values given by the EDX analysis.

$$F(D_j) = \sum_{i=1}^{n}\left[C_i^S - (C_i^S - C_i^0)erf\left(\frac{x_i}{2\sqrt{D_j\tau}}\right) - C_i(x,\tau)\right]^2 = \min. \tag{4}$$

To find the minimum of the functional 4, it is necessary to equate its first partial derivative with respect to the diffusion coefficient to zero:

$$\begin{aligned} \frac{\partial F(D_j)}{\partial D_j} =& 2\sum_{i=1}^{n}\left[C_i^S - (C_i^S - C_i^0)erf\left(\frac{x_i}{2\sqrt{D_j\tau}}\right) - C_i(x,\tau)\right] \\ &\times \exp\left(-\frac{x_i^2}{4D_j\tau}\right)\cdot(C_i^S - C_i^0)\cdot\frac{x_i}{2\sqrt{D_j^3\tau}}. \end{aligned} \tag{5}$$

$$\sum_{i=1}^{n}\left(C_i^S - C_i(x,\tau)\right)\cdot x_i\cdot\exp\left(-\frac{x_i^2}{4D_j\tau}\right) - (C_i^S - C_i^0)\sum_{i=1}^{n}x_i\exp\left(-\frac{x_i^2}{4D_j\tau}\right)erf\left(\frac{x_i}{2\sqrt{D_j\tau}}\right) = 0. \tag{6}$$

down the diffusion of carbon and vice versa. In this case, diffusion can be described by the model described below.

The classical diffusion equation is solved:

Table 1 Diffusion coefficients D of carbon and nitrogen without taking into account the interaction of flows of diffusing atoms

Diffuser	D (μm²/s)
Carbon	0.998 ± 0.015
Nitrogen	0.461 ± 0.007

Equation (6) is not solved analytically, the results of its graphical solution are shown in Table 1.

Nitrogen and carbon atoms in the process of nitrocarburising diffuse into the iron matrix simultaneously. Diffuser flows can either accelerate or slow down the diffusion of each other. It is possible to describe the effect of diffusion of nitrogen atoms on the diffusion of carbon atoms and vice versa by solving the system of interdependent differential Eqs. (7) instead of independent Eqs. (1):

$$\frac{\partial c_i}{\partial \tau} = \sum_{m=1}^{N} D_{im} \frac{\partial^2 c_m}{\partial x^2} \qquad (7)$$

The off-diagonal diffusion coefficients in systems of interrelated Eqs. (7) describe the mutual influence of the fluxes of diffusant atoms on each other.

The general form of the initial and boundary conditions for the differential equation of the second order in the coordinate and the first in time remains the same:

$$c_i(x,0) = c_i^0;$$
$$c_i(0,\tau) = c_i'; \qquad (8)$$
$$c_i(\infty,\tau) = c_i^0.$$

To simplify the solution, the system of interdependent Eqs. (7) will be reduced to a system of independent equations using the following actions:

Instead of $c_i(x,\tau)$, we introduce the functions $y_i(x,\tau)$ in accordance with the equality:

$$y_i(x,\tau) = c_i(x,\tau) - c_i' . \qquad (9)$$

Substitution of functions (9) into the system of Eqs. (7) gives a system of relatively new functions:

$$\frac{\partial y_i}{\partial \tau} = \sum_{m=1}^{N} D_{im} \frac{\partial^2 y_m}{\partial x^2}, \qquad (10)$$

The initial and boundary conditions change to:

$$y_i(x,0) = c_i^0 - c_i' = B_i;$$
$$y_i(0,\tau) = 0; \qquad (11)$$
$$y_i(\infty,\tau) = c_i^0 - c_i' = B_i.$$

We multiply both sides of Eq. (10) by some constant factors a_{ij} and sum over the second index:

$$\sum_{j=1}^{N} a_{ij} \frac{\partial y_i}{\partial \tau} = \sum_{j=1}^{N} a_{ij} \sum_{m=1}^{N} D_{jm} \frac{\partial^2 y_m}{\partial x^2} = \sum_{m=1}^{N} \left(\sum_{j=1}^{N} a_{ij} D_{jm} \right) \frac{\partial^2 y_m}{\partial x^2} \qquad (12)$$

This let us require the following condition for the matrix element a_{ij}:

$$\sum_{j=1}^{N} a_{ij} D_{jm} = D_i a_{im} , \qquad (13)$$

and using a matrix of elements a_{ij}, we introduce the functions Y_i, which will allow us to decouple the system of interdependent Eqs. (10):

$$Y_i(x,\tau) = \sum_{m=1}^{N} a_{im} y_m(x,\tau) , \qquad (14)$$

and obtain a new system of independent equations

$$\frac{\partial Y_i}{\partial \tau} = D_i \frac{\partial^2 Y_i}{\partial x^2} \qquad (15)$$

with initial and boundary conditions:

$$Y_i(x,0) = B_i \sum_{m=1}^{N} a_{im};$$
$$Y_i(0,\tau) = 0; \qquad (16)$$
$$Y_i(\infty,\tau) = B_i \sum_{m=1}^{N} a_{im}.$$

Solutions to system (15) with conditions (16) are known through the error function and have the form:

$$Y_i(x,\tau) = B_i \left(\sum_{m=1}^{N} a_{im} \right) erf\left(\frac{x}{2\sqrt{D_i \tau}} \right). \qquad (17)$$

Denote:

$$k_i = \frac{1}{2\sqrt{D_i \tau}}. \qquad (18)$$

We substitute the notation (18) into (17):

$$Y_i(x,\tau) = B_i \left(\sum_{m=1}^{N} a_{im} \right) erf(k_i x). \qquad (19)$$

The expressions for the Y_i function (14) and (19) allow us to assume that:

$$\sum_{m=1}^{N} a_{im} \left[y_m(x,\tau) - B_i erf(k_i x) \right] = 0. \qquad (20)$$

For a certain given point in time and experimental concentration values at known points, we obtain a system of equations:

$$\sum_{m=1}^{N} a_{im} \left[y_m(x_k) - B_i erf(k_i x_k) \right] = 0, \qquad (21)$$

which is resolvable at $a_{im} \neq 0$ if:

$$\left| y_m(x_k) - erf(k_i x_k) \right| = 0. \tag{22}$$

In the last formula, only k_i is unknown, so it can be considered as a system of equations for determining k_i.

Calculations for a system with interdependent diffusion of nitrogen and carbon will yield:

$$erf(kx_1)\left[y_2(x_2) - y_1(x_2)\frac{B_2}{B_1} \right] - erf(kx_2)\left[y_2(x_1) - y_1(x_1)\frac{B_2}{B_1} \right] =$$
$$\frac{1}{B_1} \begin{vmatrix} y_1(x_1) & y_2(x_1) \\ y_1(x_2) & y_2(x_2) \end{vmatrix} \tag{23}$$

By solving Eq. (23) one can find two different roots k_1, k_2, and then, using (18), determine two values D_1, D_2. Then, for known k, from Eq. (21) we find a_{im}.

$$a_{11}\left[y_1(x_1) - B_1 erf(k_1 x_1) \right] + a_{12}\left[y_2(x_1) - B_2 erf(k_1 x_1) \right] = 0$$
$$a_{11}\left[y_1(x_2) - B_1 erf(k_1 x_2) \right] + a_{12}\left[y_2(x_2) - B_2 erf(k_1 x_2) \right] = 0 \tag{24}$$

From system (24) $a_{11}/a_{12} = m$ is found:

$$a_{21}\left[y_1(x_1) - B_1 erf(k_2 x_1) \right] + a_{22}\left[y_2(x_1) - B_2 erf(k_2 x_1) \right] = 0$$
$$a_{21}\left[y_1(x_2) - B_1 erf(k_2 x_2) \right] + a_{22}\left[y_2(x_2) - B_2 erf(k_2 x_2) \right] = 0 \tag{25}$$

From system (25) $a_{21}/a_{22} = n$ is found:

Further, from system (13), the diffusion coefficients are found (Table 2):

$$D_{11} = \frac{mD_1 - nD_2}{m - n}$$
$$D_{12} = \frac{D_1 - D_2}{m - n}$$
$$D_{21} = \frac{mn(D_2 - D_1)}{m - n} \tag{26}$$
$$D_{22} = \frac{mD_2 - nD_1}{m - n}$$

The diagonal diffusion coefficient D_{11} shows how carbon would diffuse if there were no other diffusion fluxes. The influence of the flow of nitrogen atoms on the diffusion of carbon is shown by the off-diagonal coefficient D_{12}. The off-diagonal coefficient is positive, which means that nitrogen accelerates the diffusion of carbon in austenite, increasing its thermodynamic activity. The diagonal coefficient D_{22} characterizes the intrinsic diffusion of nitrogen without taking into account the influence of carbon diffusion on it. The cross off-diagonal diffusion coefficient D_{21} is positive and shows that the diffusion of nitrogen is in turn also accelerated by the parallel diffusion of carbon.

Positive values of cross diffusion coefficients mean a mutual increase in the thermodynamic activity of diffusants in austenite (at the diffusion saturation temperature, the steel will have an austenitic structure), associated with their physical displacement of each other.

The consequence of diffusion saturation of the surface layer and quenching is an increase in microhardness up to 1020 ± 20 HV (Fig. 4), associated with the formation of martensite [20]. With an increase in the PENC duration, the thickness of the hardened zone increases.

3.2 Morphology and Roughness of the Surface

The PENC of low-carbon steel in an aqueous solution leads to the formation of a typical surface morphology after cathodic treatment—the formation of a non-constant thickness of the oxide layer with cracks and pores (Fig. 5). The destruction of the surface oxide layer by discharges contributes to the removal of the material, which manifests itself in a linear decrease in the weight of samples and nonlinear dependence of roughness on the processing time (Table 3). The complex dependence of roughness on processing time is associated with the action of two processes: oxidation with the formation of an oxide layer and destruction by discharges. If the discharges act primarily on the protrusions, removing them and the resulting oxide phases, then the accumulation of oxidation products occurs in the depressions. Thus, the destructive effect of discharges, which occurs quickly, is compensated by slower oxidation.

The subsequent anodic PEP of nitrocarburised samples was carried out after 30 min of saturation, when the surface layer was subjected to greater diffusion saturation and had the greatest thickness and microhardness. As a result of polishing, a decrease in surface roughness to the initial value is observed (Table 3). The change in surface morphology manifests itself in the removal of the outer loose part of the oxide layer (Fig. 5). It should be noted that an increase in the PEP time from 1 to 2 min does not lead to a greater decrease in roughness.

3.3 Surface Friction and Wear Characteristics

According to the results of tribological tests, it was revealed that with an increase in the treatment time, a decrease in the coefficient of friction and weight wear occurs (Table 3, Fig. 6), which correlates with a decrease in surface roughness, favoring sliding of the counter body over the surface, and an increase in the thickness of the hardened

Table 2 Diffusion coefficients of carbon and nitrogen, taking into account the interaction of flows of diffusing atoms

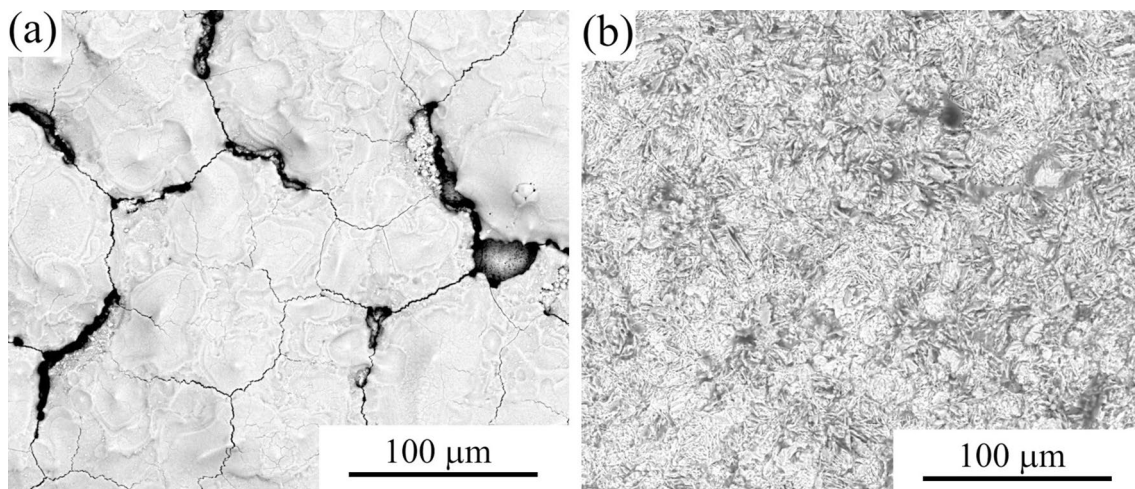| Diffuser		D ($\mu m^2/s$)
Carbon	D_{11}	0.983 ± 0.015
	D_{12}	0.138 ± 0.020
Nitrogen	D_{21}	0.710 ± 0.011
	D_{22}	0.318 ± 0.005

Fig. 5 Morphology of the steel surface after cathodic PENC for 30 min (**a**) and subsequent anodic PEP for 1 min (**b**)

Table 3 Conditions of PENC and PEP and results of samples testing. Friction tests were carried out in dry friction mode under a load of 10 N. The sliding speed of the sample along the counter body was 1.555 m/s. The sliding distance was 1000 m

| Treatment time (min)	Weight loss of samples during treatment (mg)	Surface roughness Ra (µm)	Average friction coefficient for the last 100 m of track	Weight loss of samples during tribological test (mg)
Untreated	–	1.00 ± 0.10	0.824 ± 0.015	14.0 ± 0.3
PENC 5	67 ± 11	2.34 ± 0.30	0.541 ± 0.011	13.4 ± 0.2
PENC 10	139 ± 6	1.98 ± 0.23	0.484 ± 0.009	12.1 ± 0.2
PENC 20	276 ± 14	1.43 ± 0.13	0.475 ± 0.009	10.4 ± 0.2
PENC 30	416 ± 24	1.29 ± 0.17	0.461 ± 0.009	7.2 ± 0.1
PENC 30 + PEP 1	12 ± 2	0.98 ± 0.12	0.396 ± 0.006	0.6 ± 0.1
PENC 30 + PEP 2	14 ± 2	1.00 ± 0.11	0.419 ± 0.006	10.8 ± 0.2
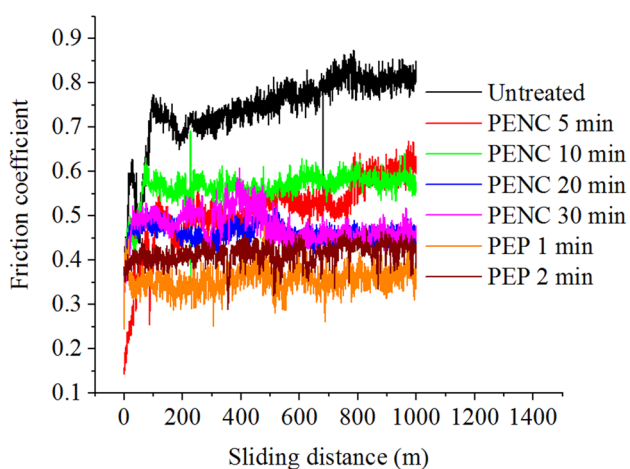
Fig. 6 The dependence of the friction coefficient on the sliding distance of the untreated sample and samples after cathodic PENC for 5, 10, 20, and 30 min and subsequent anodic PEP for 1 and 2 min. The load and sliding speed were 10 N and 1.555 m/s

nitrocarburised layer. Despite the fact that the roughness of the nitrocarburised surface is higher than that of the untreated sample, the resulting oxide layer during PENC will act as a friction lubricant, compensating for the high surface roughness. The subsequent PEP of nitrocarburised samples shows a decrease in roughness to the initial value and, accordingly, a decrease in the friction coefficient by 2 times and weight wear by 23 times compared to the untreated surface.

On samples polished for 1 min after cathodic PENC, the effect of tribological test conditions on wear characteristics was studied. An analysis of the surface of the friction tracks after duplex treatment indicates the absence of traces of microcutting (abrasive wear), which confirms the good antifriction properties of the modified steel (Fig. 7). EDX analysis shows an increased content of chemical elements on the surface, which are part of the counter body (Table 4). At the same time, their content on the treated sample is higher
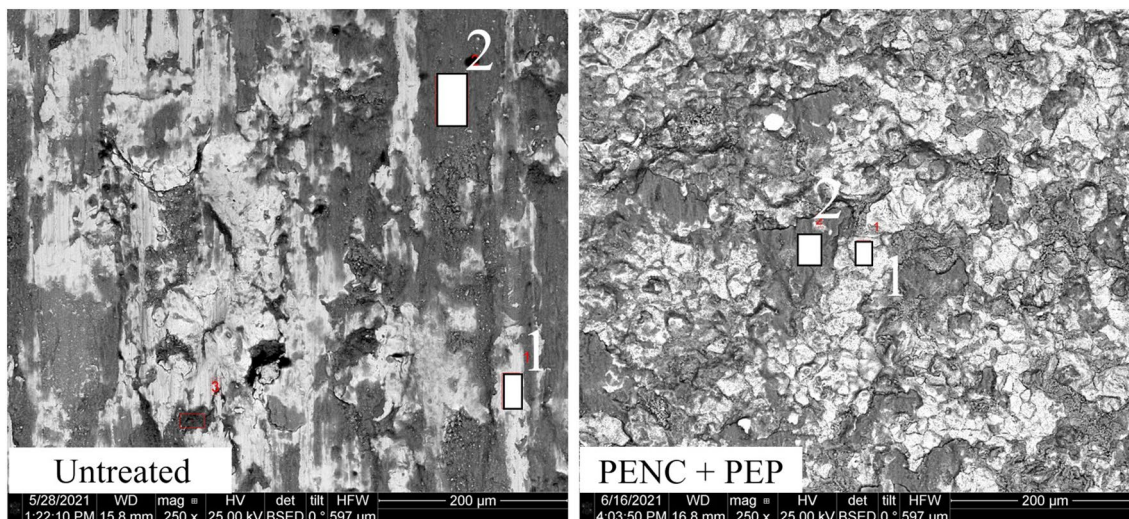
Fig. 7 SEM image of wear tracks of the surface untreated sample and duplex treated sample (cathodic PENC for 30 min and subsequent anodic PEP for 1 min). The load, sliding speed and distance were 10 N, 1.555 m/s and 1000 m, respectively

Table 4 Elemental composition (wt.%) of some areas of the friction track (Fig. 7)

Element	Untreated sample		Duplex treated sample	
	Scanning area			
	1	2 (oxidation zone)	1	2 (oxidation zone)
C	1.35 ± 0.15	1.45 ± 0.14	0.64 ± 0.17	1.01 ± 0.19
N	–	–	0.40 ± 0.16	–
O	8.70 ± 0.19	36.34 ± 0.33	9.39 ± 0.26	31.32 ± 0.44
Si	0.35 ± 0.06	0.70 ± 0.05	0.54 ± 0.08	1.04 ± 0.08
Cr	0.08 ± 0.04	0.36 ± 0.04	0.13 ± 0.05	0.35 ± 0.06
Mn	0.52 ± 0.06	0.30 ± 0.05	0.62 ± 0.08	0.35 ± 0.08
Ni	0.19 ± 0.07	0.05 ± 0.06	0.29 ± 0.11	0.26 ± 0.10
Cu	0.05 ± 0.09	-	0.13 ± 0.11	0.11 ± 0.10
Fe	Total 100	Total 100	Total 100	Total 100

Fig. 8 The dependence of the weight loss during friction of the duplex treated samples and counter body (cathodic PENC for 30 min and subsequent anodic PEP for 1 min) on the load. The sliding speed and distance were 1.555 m/s and 1000 m

than on the untreated one. This indicates a greater wear resistance of the steel surface after duplex treatment.

The influence of the load on friction and wear depends on the type of contact interaction of rubbing surfaces—elastic, plastic or elastoplastic. It is shown that the amount of weight wear is proportional to the load both for the sample and for the counter body (Fig. 8). Under conditions of predominance of plastic deformation over elastic in tribocoupling, the actual area of contact is directly proportional to the load (Fig. 9). Wear occurs on the actual area of contact, and, therefore, increases with increasing load. As the load increases, the volume of the surface layers of the material drawn into the deformation increases, which leads to an increase in the amount of heat released during friction (Fig. 10). The adhesive component of the friction coefficient
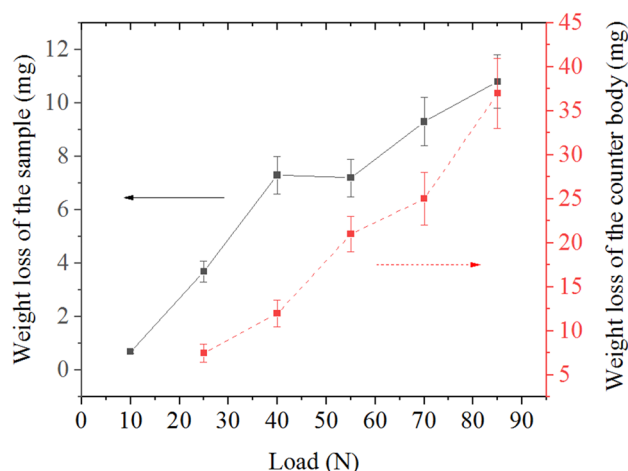
is inversely proportional to the actual contact pressure. In plastic contact, the actual pressure is equal to the hardness of the material with least hardness among the contacting materials, and does not depend on the load. The deformation component of the friction coefficient is proportional to the kinetic introduction of irregularities and for a single irregularity is determined by the force of resistance to plastic deformation of the friction surface. With plastic contact, the mutual penetration of irregularities increases with increasing load, which means that the deformation component of the friction force also increases. Taking into account that the adhesion component of the friction coefficient is equal to a constant, the total friction coefficient increases with an
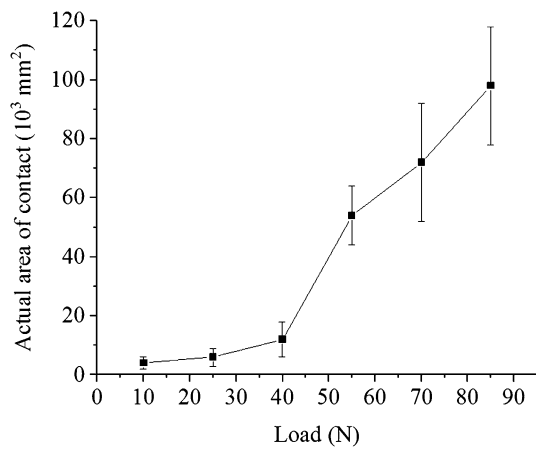
Fig. 9 The dependence of the actual area of contact during friction of the duplex treated samples (cathodic PENC for 30 min and subsequent anodic PEP for 1 min) on the load. The sliding speed and distance were 1.555 m/s and 1000 m
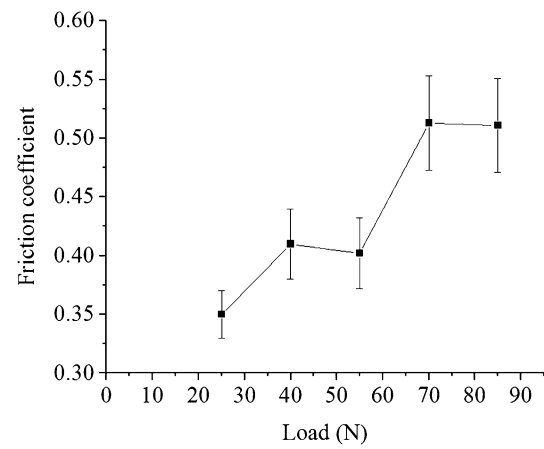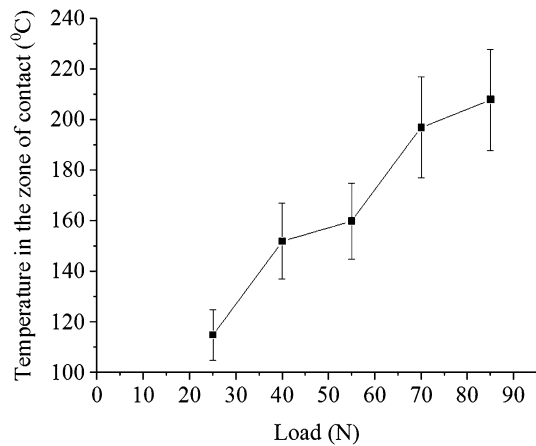

Fig. 11 The dependence of the friction coefficient of the duplex treated samples (cathodic PENC for 30 min and subsequent anodic PEP for 1 min) on the load. The sliding speed and distance were 1.555 m/s and 1000 m

Fig. 10 The dependence of temperature in the zone of frictional contact during friction of the duplex treated samples (cathodic PENC for 30 min and subsequent anodic PEP for 1 min) on the load. Temperature of the untreated sample was (80 ± 3) °C. The sliding speed and distance were 1.555 m/s and 1000 m
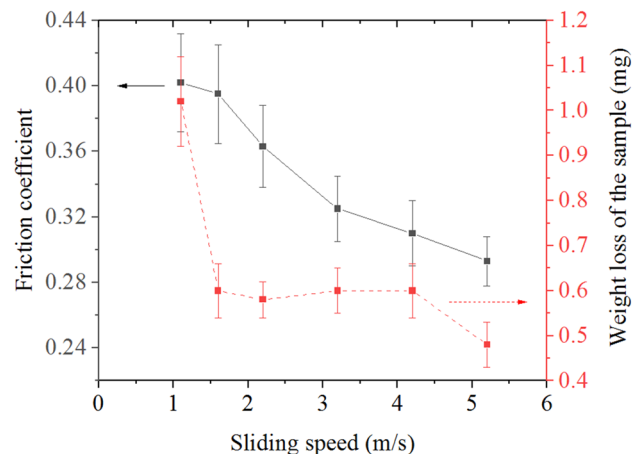

Fig. 12 The dependence of the friction coefficient and weight loss of the duplex treated samples (cathodic PENC for 30 min and subsequent anodic PEP for 1 min) on the sliding speed. The load and sliding distance were 10 N and 1000 m

increase in the load under plastic deformations in the tribo-coupling (Fig. 11). With increasing load, the wear intensity increases with plastic contact. In plastic contact, the sliding speed can affect friction through the rate of propagation of plastic deformation. With an increase in the sliding speed, plastic deformation is localized in a smaller near-surface volume, and the friction coefficient and weight wear (Fig. 12) decrease. Based on the foregoing, it has been established that the wear mechanism of modified samples is fatigue wear during boundary friction and plastic contact.

4 Conclusions

1. The possibility of increasing the wear resistance of low-carbon steel by duplex plasma electrolytic treatment combining cathodic nitrocarburising and anodic polishing is shown.
2. The composition and structure of the modified layer formed during duplex treatment, which is a surface oxide layer and a hardened to 1020 ± 20 HV nitrocarburised layer under it, have been studied.

3. Anodic polishing improves the surface morphology by removing irregularities and weak areas of the oxide layer.

4. The complex effect of surface roughness and morphology, the hardness of the diffusion layer on the tribological properties of the treated surface has been established.

5. It is revealed that the wear mechanism of modified samples is fatigue wear under boundary friction and plastic contact.

References

1. Yerokhin A L, Nie X, Leyland A, Matthews A, and Dowey S, *Surf Coat Technol* **122** (1999) 73. https://doi.org/10.1016/S0257-8972(99)00441-7.

2. Aliofkhazraei M, Macdonald D D, Matykina E, Parfenov E V, Egorkin V S, Curran J A, Troughton S C, Sinebryukhov S L, Gnedenkov S V, Lampke T, Simchen F, and Nabavi H F, *Appl Surf Sci Adv* **5** (2021) 100121. https://doi.org/10.1016/j.apsadv.2021.100121.

3. Jin S, Ma X, Wu R, Wang G, Zhang J, Krit B, Betsofen S, and Liu B, *Appl Surf Sci Adv* **8** (2022) 100219. https://doi.org/10.1016/j.apsadv.2022.100219.

4. Bogdashkina N L, Gerasimov M V, Zalavutdinov R K, Kasatkina I V, Krit B L, Lyudin V B, Fedichkin I D, Shcherbakov A I, and Apelfeld A V, *Surf Eng Appl Electrochem* **54** (2018) 331. https://doi.org/10.3103/S106837551804004X.

5. P.N. Belkin, S.A. Kusmanov, and E.V. Parfenov, *Appl Surf Sci Adv* **1** (2020) 100016. DOI: https://doi.org/10.1016/j.apsadv.2020.100016.

6. Belkin P N, Yerokhin A L, and Kusmanov S A, *Surf Coat Technol* **307** (2016) 1194. https://doi.org/10.1016/j.surfcoat.2016.06.027.

7. Belkin V S, Belkin P N, Krit B L, Morozova N V, and Silkin S A, *J Mat Eng Perform* **29** (2020) 564. https://doi.org/10.1007/s11665-019-04521-1.

8. Kusmanov S A, Kusmanova Y V, Smirnov A A, and Belkin P N, *Mat Chem Phys* **175** (2016) 164171. https://doi.org/10.1016/j.matchemphys.2016.03.011.

9. Rastkar A R, and Shokri B, *Surf Interface Anal* **44** (2012) 342. https://doi.org/10.1002/sia.3808.

10. Tsotsos C, Yerokhin A L, Wilson A D, and Leyland A, *Wear* **253** (2002) 986. https://doi.org/10.1016/S0043-1648(02)00225-9.

11. Kazerooniy N A, Bahrololoom M E, Shariat M H, Mahzoon F, and Jozaghi T, *J Mater Sci Technol* **27** (2011) 906. https://doi.org/10.1016/S1005-0302(11)60163-1.

12. Skakov M, Rakhadilov B, Scheffner M, Karipbaeva G, and Rakhadilov M, *Appl Mech Mater* **379** (2013) 161. https://doi.org/10.4028/www.scientific.net/AMM.379.161.

13. Skakov M, Verigina L, and Scheffner M, *Appl Mech Mater* **698** (2015) 439. https://doi.org/10.4028/www.scientific.net/AMM.698.439.

14. Zarchi M K, Shariat M H, Dehghan S A, and Solhjoo S, *J Mater Res Technol* **2** (2013) 213. https://doi.org/10.1016/j.jmrt.2013.02.011.

15. Jiang Y F, Geng T, Bao Y F, and Zhu Y, *Surf Coat Technol* **216** (2013) 232. https://doi.org/10.1016/J.SURFCOAT.2012.11.050.

16. Kusmanov S A, Silkin S A, Smirnov A A, and Belkin P N, *Wear* **386** (2017) 239. https://doi.org/10.1016/j.wear.2016.12.053.

17. Kusmanov S A, Tambovskiy I V, Korableva S S, Dyakov I G, Burov S V, and Belkin P N, *J Mat Eng Perform* **28** (2019) 5425. https://doi.org/10.1007/s11665-019-04342-2.

18. Smirnov A A, Kusmanov S A, Kusmanova I A, and Belkin P N, *Surf Eng Appl Electrochem* **53** (2017) 413–418. https://doi.org/10.3103/S106837551705012X.

19. Mukhacheva T L, Kalinina T M, and Kusmanov S A, *J Phys Conf Ser* **2144** (2021) 012031. https://doi.org/10.1088/1742-6596/2144/1/012031.

20. Mukhacheva T L, Belkin P N, Dyakov I G, and Kusmanov S A, *Wear* **462** (2020) 203516. https://doi.org/10.1016/j.wear.2020.203516.